Ultrafast Intramolecular Relaxation and Wave-Packet Motion in a Ruthenium-Based Supramolecular Photocatalyst

Maria Wächtler,[a, b] Julien Guthmuller,[c] Stephan Kupfer,[b] Margherita Maiuri,[d] Daniele Brida,[e] Jürgen Popp,[a, b] Sven Rau,[f] Giulio Cerullo,[d] and Benjamin Dietzek*[a, b, g]

Received: December 4, 2014
Published online on March 20, 2015

Nonequilibrium vibrational dynamics play a key role in the ultrafast photophysics of natural systems, for example, light-harvesting antennae and reaction centers,[1] or in the primary photochemical event of vision.[2] A hotly debated question is whether such nonequilibrium vibrational dynamics could also influence the efficiency of artificial photosynthetic systems, due to the potential to promote energy or electron transfer and/or coherently drive the formation of photoproducts. Hence, the analysis of vibrational coherences prepared upon impulsive excitation can shed light on the photoreaction mechanisms.[2a,3] An important paradigm for artificial light-harvesting systems is based on light-absorbing transition-metal complexes, especially ruthenium–polypyridine dyes, coupled to electron and/or energy acceptors.[4] Despite the large number of investigations dealing with ultrafast processes in ruthenium–polypyridine complexes, only few studies report specifically on the observation of vibrational coherences. These reports include studies on RuN3 in solution and adsorbed onto TiO_2 surfaces,[5] observation of nuclear coherences in a highly strained halogenated Ru–terpyridine complex,[6] and investigation of the possible impact of specific nuclear motions on photoinduced processes, for example, electron injection into TiO_2.[7]

Following the general relaxation scheme for homoleptic Ru^{2+} diimine complexes, for example, $[Ru(bpy)_3]^{2+}$ (bpy = 2,2′-bipyridine), excitation into the ^{1}MLCT manifold triggers an ultrafast intramolecular relaxation, that is, co-occurring internal conversion (IC), internal vibrational energy redistribution (IVR), and intersystem crossing (ISC), which leads to the population of the manifold of vibrationally hot triplet states approximately within the first 200 fs with a quantum yield close to unity.[8] Exact ISC times, which were determined by fluorescence upconversion experiments, are in the range of $\tau \leq 40$ fs.[9] This process is followed by vibrational relaxation to the lowest thermally relaxed ^{3}MLCT state within a few ps.[3f,4,8d–f,9b,c,10] In heteroleptic metal complexes and complexes containing more extended ligand systems additional interligand electron transfer (ILET) processes and low-lying intraligand (IL) states become accessible for population.[3f,8c,d,11] Further relaxation pathways depend, according to the excitation wavelength, on the char-

[a] *M. Wächtler, J. Popp, B. Dietzek*
Leibniz-Institute of Photonic Technology Jena (IPHT) e.V. Albert-Einstein-Str. 9, 07745, Jena (Germany)
Fax: (+49) 3641-206390
E-mail: benjamin.dietzek@ipht-jena.de

[b] *M. Wächtler, S. Kupfer, J. Popp, B. Dietzek*
Institute of Physical Chemistry and Abbe Center of Photonics Friedrich-Schiller University Jena
Helmholtzweg 4, 07743 Jena (Germany)

[c] *J. Guthmuller*
Faculty of Applied Physics and Mathematics
Gdańsk University of Technology
Narutowicza 11/12, 80233 (Poland)

[d] *M. Maiuri, G. Cerullo*
IFN-CNR, Dipartimento di Fisica, Politecnico di Milano Piazza Leonardo da Vinci 32, 20133, Milano (Italy)

[e] *D. Brida*
Department of Physics and Center for Applied Photonics
University of Konstanz, 78457 Konstanz (Germany)

[f] *S. Rau*
Institute of Inorganic Chemistry I, University of Ulm
Albert-Einstein-Allee 11, 89081 Ulm (Germany)

[g] *B. Dietzek*
Humboldtstr. 10, 07743, Jena (Germany), and
Center for Energy and Environmental Chemistry (CEEC) Jena
Philosophenweg 7a, 07743 Jena (Germany)

acteristics of the Franck-Condon (FC) state (nature of the electronic state and/or amount of excess vibrational energy), as suggested by the observation of dual emission and excitation-wavelength-dependent quantum yields.[8c,d,f,12]

In this work we apply transient absorption (TA) spectroscopy to the study of the ultrafast relaxation processes and the coherent wave-packet dynamics in the supramolecular photocatalyst RutpphzPd, with a previously inaccessible sub-20 fs time resolution. RutpphzPd ($[(tbbpy)_2Ru(tpphz)PdCl_2]^{2+}$, tpphz = tetrapyrido[3,2-a:2′,3′-c:3″,2″-h:2‴,3‴-j]phenazine, tbbpy = 4,4′-di-*tert*-butyl-2,2′-bipyridine; Figure 1 A) is one of the first reported supramolecular systems capable of evolving hydrogen upon irradiation in the presence of a sacrificial electron donor (e.g., triethylamine).[13] Based on TA spectroscopy it was shown that the catalytic mechanism in RutpphzPd comprises two photoinduced reduction steps:[14] following photoexcitation, the system relaxes into ^{3}MLCT states centered on the phenanthroline (phen) part of the tpphz ligand, which involves ILET from Ru→tbbpy ^{3}MLCT states. Subsequently, the Ru→phen ^{3}MLCT state decays to a phenazine (phz) centered state ($\tau \approx 5$ ps) from which the excitation is transferred to the $PdCl_2$ moiety with a time constant of 310 ps.

One intriguing property of RutpphzPd catalysis is the excitation-wavelength-dependent efficiency, which has been correlated to the nature of the initial excited state in the first photoreduction step:[15] a higher catalytic efficiency is observed upon excitation in the red wing of the ^{1}MLCT absorption band (Ru→tpphz ^{1}MLCT transition) than upon excitation at shorter wavelengths, where Ru→tbbpy ^{1}MLCT excitations show stronger contributions to the overall absorbance, which was shown by resonance Raman spectroscopy[15a] and theoretical investigations[15a,16] (Table 1). This behavior is more closely examined herein. Here, particular emphasis is on the impact of coordination of the catalytic Pd^{II} center on the ultrafast photoinduced processes. In former investigations it has been shown that the Pd^{II} center has a great impact on the excited-state manifold, modifying the lifetimes and spectral characteristics of the system, for example, a redshift of the ^{1}MLCT transition to the tpphz bridge is observed upon coordination of the Pd^{II} center (Figure 1 and Table 1).[14] Further, differences in the resonance

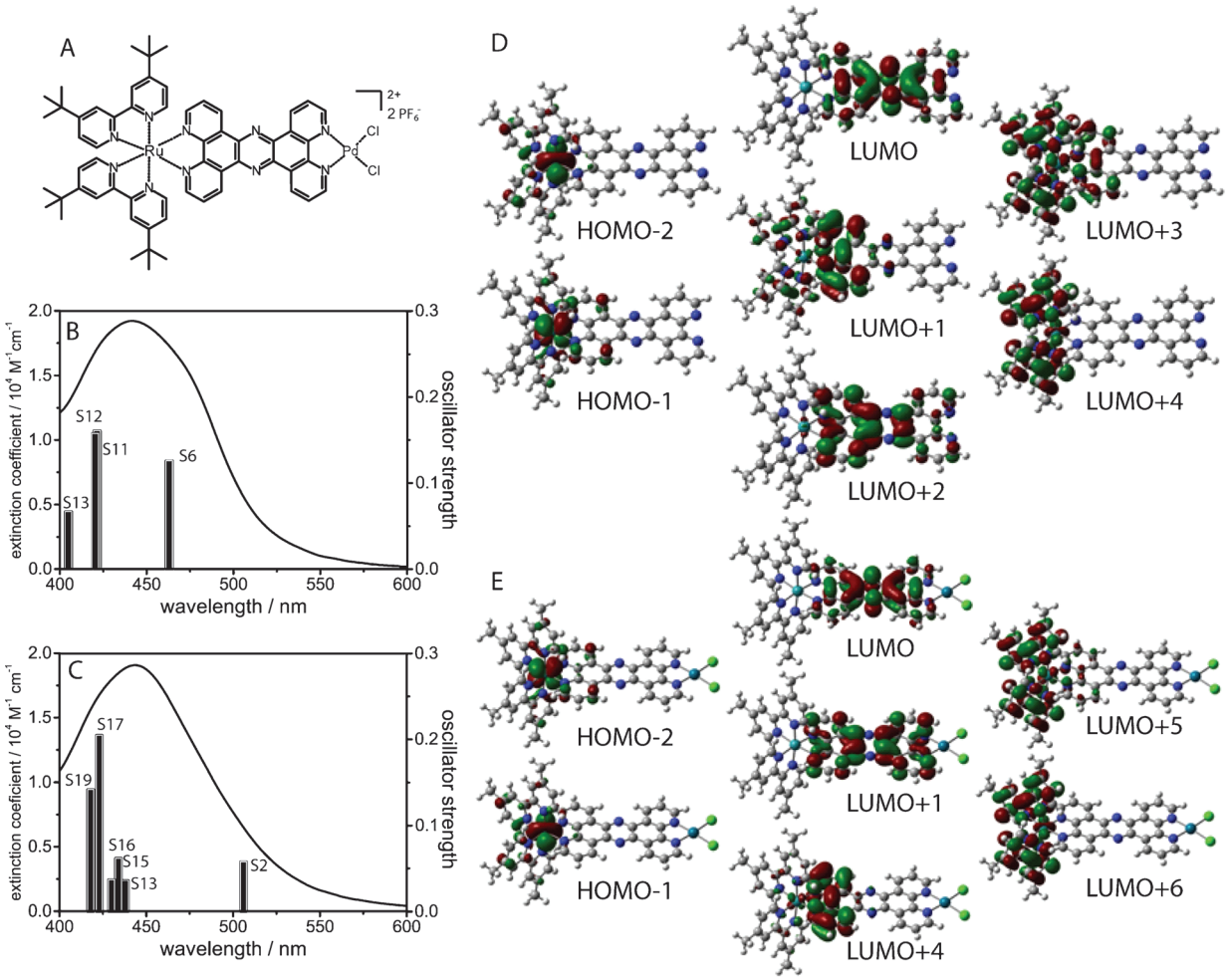

Figure 1. A) Molecular structure of the investigated photocatalyst RutpphzPd. Experimental absorption spectra in acetonitrile (solid line) are given in conjunction with the oscillator strength for the calculated electronic transitions (stick plot) contributing to the ^{1}MLCT band in the visible spectral range for B) Rutpphz and C) RutpphzPd. Molecular orbitals of D) Rutpphz and E) RutpphzPd with contributions to the electronic configurations, which describe the electronic excited states (Table 1).

Table 1. Singlet excitation energies of RutpphzPd and Rutpphz calculated at the ground-state geometry (TDDFT/B3LYP). Only transitions with an oscillator strength $f > 0.01$ are displayed.

State	Transition	Weight [%]	E [eV]	λ [nm]	f
Rutpphz					
S6 (S_{phz})	d_{Ru}(HOMO-1)→π^*_{tpphz}(LUMO)	82	2.68	463	0.126
	d_{Ru}(HOMO-1)→ π^*_{tpphz}(LUMO + 1)	11			
S11	d_{Ru}(HOMO-1)→ π^*_{tpphz}(LUMO + 1)	34	2.95	421	0.161
	d_{Ru}(HOMO-2)→ π^*_{tbbpy}(LUMO + 4)	25			
	d_{Ru}(HOMO-2)→ π^*_{tpphz}(LUMO + 2)	18			
	d_{Ru}(HOMO-1)→π^*_{tpphz}(LUMO)	7			
	d_{Ru}(HOMO-1)→ π^*_{tbbpy}(LUMO + 3)	7			
	d_{Ru}(HOMO)→π^*_{tpphz}(LUMO + 2)	6			
S12	d_{Ru}(HOMO-2)→ π^*_{tbbpy}(LUMO + 3)	47	2.95	421	0.158
	d_{Ru}(HOMO-1)→ π^*_{tbbpy}(LUMO + 4)	40			
	d_{Ru}(HOMO-2)→ π^*_{tpphz}(LUMO + 1)	6			
	d_{Ru}(HOMO-1)→ π^*_{tpphz}(LUMO + 2)	5			
S13	d_{Ru}(HOMO-2)→ π^*_{tpphz}(LUMO + 2)	67	3.06	405	0.067
	d_{Ru}(HOMO-2)→ π^*_{tbbpy}(LUMO + 4)	29			
RutpphzPd					
S2 (S_{phz})	d_{Ru}(HOMO-2)→π^*_{tpphz}(LUMO)	96	2.45	506	0.058
S13	d_{Ru}(HOMO-1)→π^*_{tpphz}(LUMO + 1)	67	2.83	438	0.036
	d_{Ru}(HOMO-2)→π^*_{tpphz}(LUMO + 4)	26			
S15	d_{Ru}(HOMO-2)→π^*_{tbbpy}(LUMO + 5)	41	2.86	434	0.062
	d_{Ru}(HOMO-2)→π^*_{tpphz}(LUMO + 4)	36			
	d_{Ru}(HOMO-1)→π^*_{tpphz}(LUMO + 1)	16			
S16	d_{Ru}(HOMO-2)→π^*_{tpphz}(LUMO + 1)	62	2.88	430	0.037
	d_{Ru}(HOMO-1)→π^*_{tbbpy}(LUMO + 5)	20			
	d_{Ru}(HOMO-2)→π^*_{tbbpy}(LUMO + 6)	12			
S17	d_{Ru}(HOMO-1)→π^*_{tbbpy}(LUMO + 6)	40	2.93	423	0.205
	d_{Ru}(HOMO-2)→π^*_{tbbpy}(LUMO + 5)	23			
	d_{Ru}(HOMO-2)→π^*_{tpphz}(LUMO + 4)	21			
	d_{Ru}(HOMO-1)→π^*_{tpphz}(LUMO + 1)	11			
S19	d_{Ru}(HOMO-2)→π^*_{tbbpy}(LUMO + 6)	52	72.9	418	0.142
	d_{Ru}(HOMO-1)→π^*_{tbbpy}(LUMO + 5)	44			

Raman (RR) spectra of $[(tbbpy)_2Ru(tpphz)]^{2+}$ (Rutpphz) and RutpphzPd indicate that the coordination of the second metal center already alters the FC region,[14] which is expected to be reflected in the early-stage photoinduced dynamics.

Population dynamics: The samples were excited at 500 nm in the red shoulder of the ^{1}MLCT band (corresponding to mainly Ru→tpphz ^{1}MLCT excitation) and at 450 nm addressing both Ru→tbbpy and Ru→tpphz ^{1}MLCT transitions. The TA spectra at probe wavelengths below 530 nm show contributions of ground-state bleach (GSB) and a broad excited-state absorption (ESA) band with a maximum at 600/590 nm for Rutpphz/RutpphzPd is observed at longer probe wavelengths (see the Supporting Information, Figure S1), this is in agreement with the transient spectra reported previously.[14] For both Rutpphz and RutpphzPd the ESA signal shows a fast build-up, followed by an additional slower rise over the investigated time range up to 2 ps (Figure 2 and Figure S1 and S2 in the Supporting Information). This rise is more pronounced upon short-wavelength excitation and appears to be slower

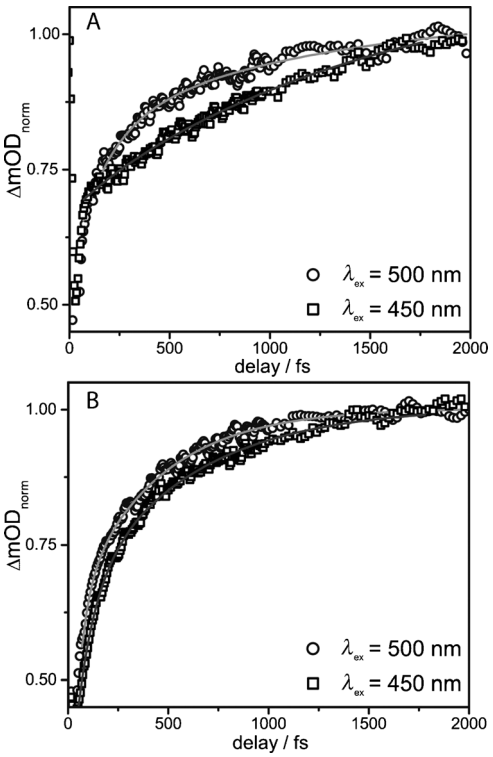

Figure 2. Ultrafast build-up of the TA signal measured with approximately 20 fs time-resolution for A) Rutpphz ($\lambda_{probe} = 600$ nm) and B) RutpphzPd ($\lambda_{probe} = 590$ nm) dissolved in acetonitrile upon excitation at 500 nm (data ○/fit line) and 450 nm (data □/fit line). At times around zero pump-probe delay strong solvent artifacts[23] are observed; these last for about 50 fs (see the Supporting Information, Figure S6) and this region was omitted in the fitting procedure.

for Rutpphz than for RutpphzPd. To quantify these observations a multiexponential fit at selected probe wavelengths delivered two kinetic components that contribute to the rise of the signal (Table 2 and Table S1 in the Supporting Information).

The slow component, τ_2, is assigned according to the model established in literature to the ILET process transferring the excitation from ^{3}MLCT states with dominating Ru→tbbpy character to states with mainly Ru→tpphz ^{3}MLCT character.[14] The previously reported time constants and the acceleration of the ILET process in RutpphzPd compared with Rutpphz are reproduced.[14] The apparent slower rise of the signal upon short-wavelength excitation is ascribed to a stronger contribution of the ILET process to the kinetics; this is also reflected in the larger amplitude, A_2. This is a consequence of the higher contributions of states with dominating Ru→tbbpy ^{1}MLCT character initially excited under these conditions and a resulting higher initial population of ^{3}MLCT states with dominating Ru→tbbpy character.

Table 2. Fit results, λ_{probe} = 600 nm Rutpphz/590 nm RutpphzPd corresponding to the respective maximum of the ESA band.[a]

	λ_{ex} [nm]	τ_1 [fs]/A_1	τ_2 [fs]/A_2
Rutpphz	500	174 ± 12/−0.277	1200/[b]−0.23
	450	200 ± 100/−0.02	1508 ± 200/−0.44
RutpphzPd	500	44 ± 6/−0.54	407 ± 11/−0.38
	450	85 ± 7/−0.38	553 ± 30/−0.48

[a] Fits for additional probe wavelengths see Table S1 in the Supporting Information; [b] The value was kept constant in the fit according to literature value.[14]

τ_1 represents the population of hot triplet states from the initially populated ^{1}MLCT states, which comprises, besides ISC, probably additional contributions from IC and IVR, which are not possible to separate from each other solely based on TA measurements.[3f,4,8d–f,9b,c] This process is slowed in both complexes upon pumping at shorter wavelengths. Additionally, τ_1 is considerably faster for RutpphzPd than for Rutpphz. As the observed process is a superposition of several contributions it is not possible to identify a single source of this deceleration. One possible explanation for the deceleration observed with shorter excitation wavelength is a slower IVR due to the increased photon energy deposited in the system that needs to be dissipated, hence, slowing down the overall process.[8f,17] Furthermore, additional IC processes in the triplet sphere might also contribute upon high energy excitation, for example, equilibration between low-lying spin–orbit states. Also, in this context it should be recognized that structural parameters may influence τ_1, as they determine the relative energetic position and the density of singlet and triplet states as well as the shape of the excited-state potential energy surfaces (PES) in the crossing region, thus impacting the vibronic coupling between the various excited states.[9c,18] This affects, not only IC and IVR, but also ISC as spin–orbit coupling (SOC) is not the only parameter governing ISC rates.[9c,18b,c,e,h] The availability of optically driven vibrational modes to explore the crossing region of PES can greatly influence the crossing rates.[18a,f–h] Hence, due to the differing localization of the initial excitation in the ligand sphere (tbbpy and/or tpphz ^{1}MLCT state), triplet population rates might differ with changing excitation conditions. The significant acceleration, by a factor of 2 to 4, of τ_1 observed for RutpphzPd compared with Rutpphz can be regarded as indication for the impact of coordination of the Pd center on the PES of the sensitizer unit or might also be related to an additional heavy atom effect enhancing SOC.

A direct observation of the presence of additional processes competing with localization in Ru→tpphz ^{3}MLCT states, which could explain the difference in the catalytic efficiency under varying excitation conditions, was not possible with the present experiment. However, the higher population of higher lying ^{3}MLCT states upon short-wavelength excitation during the first ps leads to an enhanced probability to access ^{3}MC (metal-centered) states; this offers an efficient radiationless deactivation channel.[4,19] A second possibility is an incomplete ILET, resulting in population remaining in Ru→tbbpy-dominated ^{3}MLCT states, as was observed recently for a RuPd dyad.[20] To clarify this matter the probe range needs to be extended to the near-UV region.

Coherent wave-packet motion: A closer analysis of the data reveals the presence of a coherent vibrational signature superimposed to the population dynamics of RutpphzPd, which persists beyond a delay of 1 ps (Figure 3A and Figure S3B,D in the Supporting Information). The vibrational pattern was analyzed by fast Fourier transform (FFT) analysis and was found to

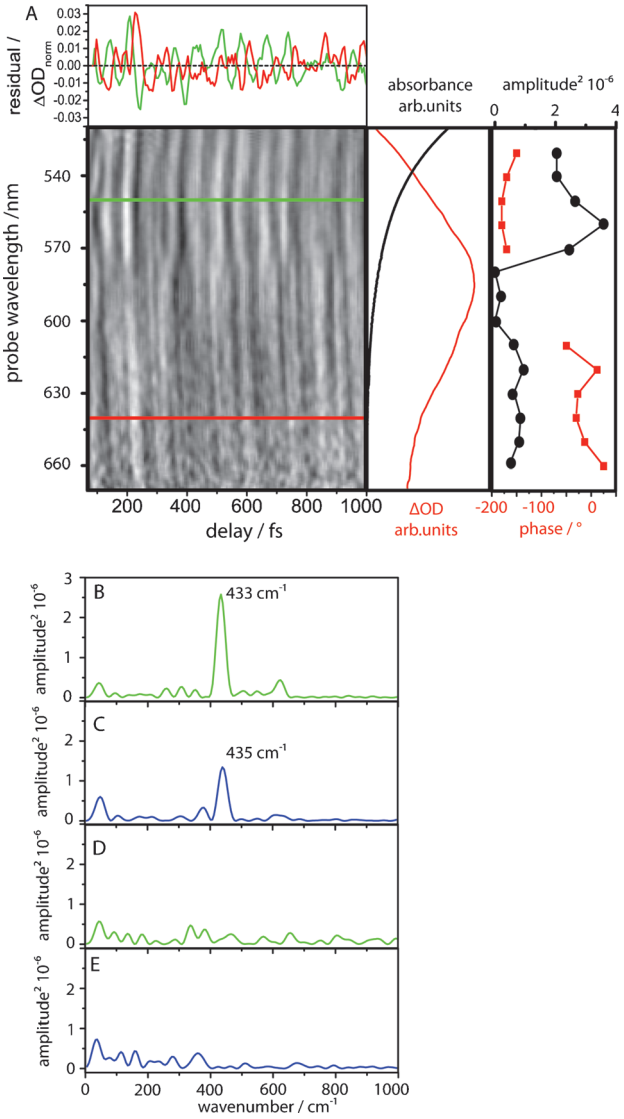

Figure 3. A) 2D map and cuts at 550 (green) and 640 nm (red) probe wavelength of the residuals (ΔOD) of the TA signal of RutpphzPd upon excitation at 500 nm after subtraction of the slow components due to population dynamics revealing the oscillatory component. Amplitude (black/dot) and phase (red/squares) profiles of the dominating approximate 433 cm^{-1} mode resulting from the FFT are displayed in parenthesis with the ground-state absorption (black) and the TA spectrum (red) at 1 ps delay time over the measured probe range. To evaluate the phase correctly a small frequency chirp of the probe pulse has to be considered (see Figures S5 and S6 in the Supporting Information).[24] The uncertainty in the phase estimation is about ±30°. FFT of the oscillatory component at 550 nm probe wavelength of RutpphzPd upon B) 500 and C) 450 nm excitation and of Rutpphz upon D) 500 and E) 450 nm excitation.

be dominated by a single oscillatory component at 433 cm^{-1} (Figure 3B). As contributions of GSB and ESA overlap in the spectral probe range, the observed oscillatory signature could be due to coherent motion in either ground or excited state. The near perfect agreement between the frequency of the oscillatory component and the frequency of a tpphz mode in the ground-state RR spectra (436 cm^{-1}; see the Supporting Information, Figure S7) is no unambiguous indication for ground-state oscillatory motion and could be accidental. However, a detailed analysis of the data upon 500 nm excitation (Figure 3A) reveals a minimum of the amplitude of the oscillatory component at the maximum of the ESA feature and a phase jump around the ESA band maximum of approximately π, which are both signatures of excited-state wave-packet motion.[2a,21] The long (>1 ps) lifetime of the oscillation implies that the coherence prepared upon excitation of the ^{1}MLCT state survives ISC and is transferred to the ^{3}MLCT state. Similar long-lived vibrational motion was reported for RuN3 in solution and attached to TiO_2[5] and for highly strained ruthenium–terpyridine complexes.[6]

Upon decreasing the excitation wavelength to 450 nm the amplitude of the oscillatory component in RutpphzPd drops (Figure 3B). Under these excitation conditions Ru→tbbpy-dominated ^{1}MLCT transitions have stronger contributions to the initial excitation.[14–15] One possible explanation for this reduced vibrational activity is that the observed coherent motion is only generated upon excitation of the Ru→tpphz ^{1}MLCT states and hence is related to a tpphz-localized vibrational mode. The absence of long-lived vibrational coherences upon excitation of higher lying ^{1}MLCT states with stronger Ru→tbbpy contributions might be connected to the observed decelerated population of the triplet manifold (longer τ_1, see Table 1), which could be an indication of differences in the coupling of higher lying singlet states to the triplet manifold; this restrains the transfer of the coherent motion to the triplet manifold. An alternative explanation would be that coherences produced upon excitation of the higher lying states have a much faster dephasing time due to coupling to other vibrations or are damped through the ILET process, which is much slower than the vibrational period and could be a source of dephasing of coherent motion. To get deeper insight into the dephasing behavior of the coherent motion under varying excitation conditions, further measurements, which extend the time range with high time resolution for observation of the decay of the oscillatory pattern, need to be performed.

In contrast to RutpphzPd, a comparable vibrational signature is completely absent in the transient signal for Rutpphz (Figure 2A and Figure S3A,C and S4A,C in the Supporting Information). The source of this effect could be significant changes in the structure of the surface crossing region and vibronic coupling between singlet and triplet manifolds induced by coordination of the Pd^{II} center. Changes in the density and nature of states available for relaxation might lead to an absence of any oscillatory signature in the Rutpphz data due to the absence of optically driven vibrational modes, which promote surface crossing and result in restrained coherence transfer to the triplet state.

Computational results: Assisted by TDDFT (time-dependent density functional theory) calculations the nature of the vibrational coordinate responsible for the observed coherent oscillation is explored. The vibrational modes in the ground and excited state in the corresponding wavenumber region are not necessarily correlated, even if located at the same frequencies, due to frequency shifts and Duschinsky rotation.[22] Hence, ground-state modes are not readily suited for reliable mode assignment in case of excited-state coherent vibration. Therefore, besides frequency calculations for the ground state, excited-state optimizations and calculations of the excited-state normal modes and frequencies are performed.

The calculation of the electronic transitions for RutpphzPd[16] (Table 1) reveals the presence of a ^{1}MLCT state (S_{phz}) with a non-negligible oscillator strength at 506 nm, which involves a transition to an acceptor orbital localized on the central phz part of the tpphz ligand (Figure 1). Upon excitation at 500 nm in resonance with S_{phz}, only one mode around 430 cm^{-1} (GS 65 at 438 cm^{-1}) is FC active, displaying a large deformation of S_{phz} with respect to the ground state (Figure 4 and Table S16 in the Supporting Information). Calculations of the normal modes for the excited state S_{phz} reveal that GS 65 corresponds mainly to a combination of the excited-state coordinates S_{phz} 65 at 437 cm^{-1} and S_{phz} 67 at 440 cm^{-1} (Figure 4 and Table S17 in the Supporting Information) along which coherent motion can be launched upon resonant excitation of S_{phz}. Because the experiments suggest that the vibrational coherence is preserved during ISC, geometry and frequency calculations were also performed for the lowest triplet state T_{phz}. The electronic character

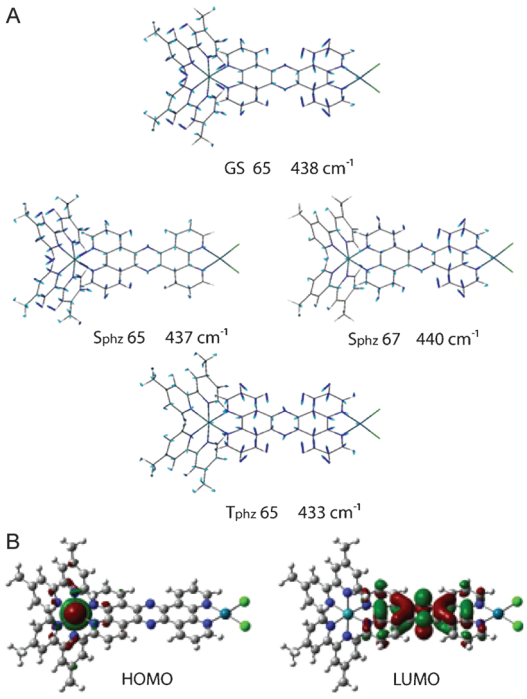

Figure 4. A) Ground-state mode and corresponding excited-state normal coordinates along which main geometry changes occur between ground state and S_{phz} or T_{phz} states and along which coherent wave-packet motion is launched upon excitation of S_{phz}. B) Molecular orbitals with main contributions to the electronic configuration of T_{phz}.

of this state resembles closely S_{phz} (Figure 4 and Table S10 and S11 in the Supporting Information). Also for T_{phz} the ground-state normal coordinate GS 65 describes a large deformation of the equilibrium geometry with respect to the ground-state geometry in the tpphz framework. Further, a normal coordinate of the excited state T_{phz} exists (T_{phz} 65), which closely resembles GS 65 (Figure 4 and Table S18 in the Supporting Information). The frequency of this triplet mode is only slightly shifted compared with the GS mode, from 438 to 433 cm^{-1}; this is in good agreement with the experimental results. Furthermore, the deformation along T_{phz} 65 going from the GS geometry (i.e., FC geometry) to the T_{phz} geometry shows the highest Δ^2 value (0.303) of all molecular modes for RutpphzPd. These results clearly point towards the outstanding role of these coordinates and it can be assumed that movement along these modes transfers the system from the FC geometry to the crossing region of PES, hence facilitating fast ISC in the nonadiabatic regime, which allows efficient transfer of the coherent motion to the triplet state.

The peculiarity of this situation becomes apparent through the absence of a distinct coordinate for higher excited states of RutpphzPd and for all excited states of Rutpphz (see the Supporting Information, Tables S16, S20, and S21). This might be caused on the one hand by the stronger mixed character of the electronic configuration of the relevant excited states, that is, mixed Ru→tpphz(phz), Ru→tpphz(phen), and Ru→tbbpy ^{1}MLCT excitations (see Table 1 and Tables S2–S15 in the Supporting Information). In these mixed states, geometry changes upon excitation are smaller and spread over several coordinates with different characters (i.e., tbbpy and tpphz modes, see the Supporting Information, Tables S16 and S20). On the other hand, the comparison of the triplet excited states below S_{phz} for RutpphzPd and Rutpphz reveals important differences. These states should participate in the relaxation to the lowest triplet state upon excitation of the S_{phz} state. In RutpphzPd, all the MLCT triplet states show similar electronic character dominated by transitions to the LUMO orbital localized on the center of the bridge and hence are expected to show comparable geometry changes as for S_{phz} and T_{phz}, that is, presence of a favorable coordinate to support the coherent motion. In the case of Rutpphz, the phz-centered ^{1}MLCT state comparable to S_{phz} in RutpphzPd is found at higher energy (463 nm). Moreover, the triplet manifold of Rutpphz below this state presents a mixed character involving transitions to the phz, phen, and tbbpy units (Figure S9 in the Supporting Information), similarly to what is found for higher excitations (above S_{phz}) in RutpphzPd (Figure S8 in the Supporting Information). These calculations support the assumption that for Rutpphz, as well as for RutpphzPd upon excitation of higher states, no favorable coordinate, which is optically active to drive the system towards the surface crossing and to support the transfer of coherence to the lowest states, is present. This absence of a distinct reactive mode might explain the loss of the coherence.

The presented results imply that the direct population of the bridge-centered state in RutpphzPd upon excitation in the red shoulder of the ^{1}MLCT absorption band gives rise to a remarkably long-lived (beyond the timescale of 1 ps) coherent wave-packet motion in the excited-state PES, which survives electronic surface crossing during ISC. The presented results indicate that this coherent nuclear motion is related to a tpphz vibrational mode, serving as a reactive mode in the photocatalytic system, bringing the system from the FC geometry into the crossing region and thereby promoting the ISC between singlet and triplet electronic surfaces through strong vibronic coupling. Due to the lack of a reactive mode upon excitation at shorter wavelengths for RutpphzPd, and for Rutpphz in general, no coherent motion in the triplet states is observed in these cases. Whether this is also related to the slower overall population of the triplet manifold or whether additional relaxation processes as IVR and IC decelerate the overall triplet population time observed here cannot be decided based on the data presented and needs further investigation. Additionally, the observation of the direct transfer of an excess charge to the center of the bridge and close to the vicinity of the Pd center upon excitation of the tpphz ^{1}MLCT state adds a new angle on the source of wavelength-dependent catalytic efficiency in this system. The presented data suggests that the catalytic efficiency of the photocatalyst depends not solely on the localization in the ligand sphere of the ruthenium center, but also further on a certain subunit of the bridging ligand. For both systems no additional processes competing with the charge localization on the tpphz ligand could be observed directly, but upon excitation at shorter wavelengths the system remains in higher excited states for a longer time; this probably enhances the probability for parallel processes, for example, the access of ^{3}MC states for radiationless relaxation, and could decrease the catalytic activity.

Acknowledgements

This work was financially supported by the Studienstiftung des deutschen Volkes (M.W.), the Fonds der Chemischen Industrie (B.D.), the 7th EU Framework Programme Marie Curie FP7 Integration Grant (J.G., Grant-No. 321971) and the Thüringer Ministerium für Bildung, Wissenschaft und Kultur (Grant-No. B 514-09049, PhotoMIC). We acknowledge support from the European Community (FP-7 INFRASTRUCTURES-2008-1, 'Laserlab Europe II', contract no. 228334) and COST Action CM1202.

[1] a) V. I. Novoderezhkin, A. G. Yakovlev, R. van Grondelle, V. A. Shuvalov, *J. Phys. Chem. B.* **2004**, *108*, 7445–7457; b) M. H. Vos, F. Rappaport, J. C. Lambry, J. Breton, J. L. Martin, *Nature* **1993**, *363*, 320–325; c) D. M. Jonas, M. J. Lang, Y. Nagasawa, T. Joo, G. R. Fleming, *J. Phys. Chem.* **1996**, *100*, 12660–12673; d) F. Fassioli, R. Dinshaw, P. C. Arpin, G. D. Scholes, *J. R. Soc. Interface* **2014**, *11*, 20130901.

[2] a) Q. Wang, R. W. Schoenlein, L. A. Peteanu, R. A. Mathies, C. V. Shank, *Science* **1994**, *266*, 422–424; b) S. L. Dexheimer, Q. Wang, L. A. Peteanu, W. T. Pollard, R. A. Mathies, C. V. Shank, *Chem. Phys. Lett.* **1992**, *188*, 61–66; c) D. Polli, P. Altoe, O. Weingart, K. M. Spillane, C. Manzoni, D. Brida, G. Tomasello, G. Orlandi, P. Kukura, R. A. Mathies, M. Garavelli, G. Cerullo, *Nature* **2010**, *467*, 440–488.

[3] a) S. Lochbrunner, A. Szeghalmi, K. Stock, M. Schmitt, *J. Chem. Phys.* **2005**, *122*, 244315; b) S. Takeuchi, T. Tahara, *J. Phys. Chem. A* **2005**, *109*, 10199–10207; c) M. Iwamura, H. Watanabe, K. Ishii, S. Takeuchi, T. Tahara, *J. Am. Chem. Soc.* **2011**, *133*, 7728–7736; d) K. Stock, C. Schriever, S. Lochbrunner, E. Riedle, *Chem. Phys.* **2008**, *349*, 197–203; e) S. Y. Kim, C. H. Kim, M. Park, K. C. Ko, J. Y. Lee, T. Joo, *J. Phys. Chem. Lett.* **2012**, *3*, 2761–2766; f) A. Vlcek, *Coord. Chem. Rev.* **2000**, *200*, 933–977.

[4] S. Campagna, F. Puntoriero, F. Nastasi, G. Bergamini, V. Balzani, *Photochemisty and Photophysics of Coordination Compounds I: Ruthenium, Vol. 280*, Springer, Berlin, **2007**.

[5] a) G. Benkö, J. Kallioinen, J. E. I. Korppi-Tommola, A. P. Yartsev, V. Sundstrom, *J. Am. Chem. Soc.* **2002**, *124*, 489 – 493; b) J. Kallioinen, G. Benko, P. Myllyperkio, L. Khriachtchev, B. Skarman, R. Wallenberg, M. Tuomikoski, J. Korppi-Tommola, V. Sundstrom, A. P. Yartsev, *J. Phys. Chem. B* **2004**, *108*, 6365 – 6373.

[6] P. J. Vallett, N. H. Damrauer, *J. Phys. Chem. A* **2013**, *117*, 6489 – 6507.

[7] B. Brüggemann, J. A. Organero, T. Pascher, T. Pullerits, A. Yartsev, *Phys. Rev. Lett.* **2006**, *97*, 208301.

[8] a) J. N. Demas, D. G. Taylor, *Inorg. Chem.* **1979**, *18*, 3177 – 3179; b) G. A. Crosby, J. N. Demas, *J. Am. Chem. Soc.* **1971**, *93*, 2841 – 2847; c) A. I. Baba, J. R. Shaw, J. A. Simon, R. P. Thummel, R. H. Schmehl, *Coord. Chem. Rev.* **1998**, *171*, 43 – 59; d) X. Y. Wang, A. Del Guerzo, R. H. Schmehl, *J. Photochem. Photobiol. C* **2004**, *5*, 55 – 77; e) N. H. Damrauer, G. Cerullo, A. Yeh, T. R. Boussie, C. V. Shank, J. K. McCusker, *Science* **1997**, *275*, 54 – 57; f) J. K. McCusker, *Acc. Chem. Res.* **2003**, *36*, 876 – 887.

[9] a) A. Cannizzo, F. van Mourik, W. Gawelda, G. Zgrablic, C. Bressler, M. Chergui, *Angew. Chem. Int. Ed.* **2006**, *45*, 3174 – 3176; *Angew. Chem.* **2006**, *118*, 3246 – 3248; b) A. C. Bhasikuttan, M. Suzuki, S. Nakashima, T. Okada, *J. Am. Chem. Soc.* **2002**, *124*, 8398 – 8405; c) M. Chergui, *Dalton Trans.* **2012**, *41*, 13022 – 13029.

[10] W. Henry, C. G. Coates, C. Brady, K. L. Ronayne, P. Matousek, M. Towrie, S. W. Botchway, A. W. Parker, J. G. Vos, W. R. Browne, J. J. McGarvey, *J. Phys. Chem. A* **2008**, *112*, 4537 – 4544.

[11] G. Benkö, J. Kallioinen, P. Myllyperkio, F. Trif, J. E. I. Korppi-Tommola, A. P. Yartsev, V. Sundstrom, *J. Phys. Chem. B* **2004**, *108*, 2862 – 2867.

[12] a) R. Siebert, A. Winter, U. S. Schubert, B. Dietzek, J. Popp, *Phys. Chem. Chem. Phys.* **2011**, *13*, 1606 – 1617; b) E. C. Glazer, D. Magde, Y. Tor, *J. Am. Chem. Soc.* **2007**, *129*, 8544 – 8551; c) T. E. Keyes, C. M. O'Connor, U. O'Dwyer, C. G. Coates, P. Callaghan, J. J. McGarvey, J. G. Vos, *J. Phys. Chem. A* **1999**, *103*, 8915 – 8920; d) R. Siebert, *Macromol. Rapid Commun.* **2010**, *31*, 883 – 888; e) P. Myllyperkiö, G. Benko, J. Korppi-Tommola, A. P. Yartsev, V. Sundstrom, *Phys. Chem. Chem. Phys.* **2008**, *10*, 996 – 1002; f) G. Singh Bindra, M. Schulz, A. Paul, R. Groarke, S. Soman, J. L. Inglis, W. R. Browne, M. G. Pfeffer, S. Rau, B. J. MacLean, M. T. Pryce, J. G. Vos, *Dalton Trans.* **2012**, *41*, 13050 – 13059.

[13] S. Rau, B. Schäfer, D. Gleich, E. Anders, M. Rudolph, M. Friedrich, H. Görls, W. Henry, J. G. Vos, *Angew. Chem. Int. Ed.* **2006**, *45*, 6215 – 6218; *Angew. Chem.* **2006**, *118*, 6361 – 6364.

[14] S. Tschierlei, M. Presselt, C. Kuhnt, A. Yartsev, T. Pascher, V. Sundström, M. Karnahl, M. Schwalbe, B. Schäfer, S. Rau, M. Schmitt, B. Dietzek, J. Popp, *Chem. Eur. J.* **2009**, *15*, 7678 – 7688.

[15] a) S. Tschierlei, M. Karnahl, M. Presselt, B. Dietzek, J. Guthmuller, L. Gonzalez, M. Schmitt, S. Rau, J. Popp, *Angew. Chem. Int. Ed.* **2010**, *49*, 3981 – 3984; *Angew. Chem.* **2010**, *122*, 4073 – 4076; b) L. Zedler, J. Guthmuller, I. R. de Moraes, S. Kupfer, S. Krieck, M. Schmitt, J. Popp, S. Rau, B. Dietzek, *Chem. Commun.* **2014**, *50*, 5227 – 5229.

[16] J. Guthmuller, L. Gonzalez, *Phys. Chem. Chem. Phys.* **2010**, *12*, 14812 – 14821.

[17] G. J. Hedley, A. Ruseckas, I. D. W. Samuel, *J. Phys. Chem. A* **2010**, *114*, 8961 – 8968.

[18] a) A. Cannizzo, A. M. Blanco-Rodriguez, A. El Nahhas, J. Sebera, S. Zalis, A. Vlcek, Jr., M. Chergui, *J. Am. Chem. Soc.* **2008**, *130*, 8967 – 8974; b) M. Etinski, V. Rai-Constapel, C. M. Marian, *J. Chem. Phys.* **2014**, *140,* 114104; c) B. R. Henry, W. Siebrand, *J. Chem. Phys.* **1971**, *54*, 1072; d) Z. A. Siddique, Y. Yamamoto, T. Ohno, K. Nozaki, *Inorg. Chem.* **2003**, *42*, 6366 – 6378; e) M. Woeller, S. Grimme, S. D. Peyerimhoff, D. Danovich, M. Filatov, S. Shaik, *J. Phys. Chem. A* **2000**, *104*, 5366 – 5373; f) W. Gawelda, A. Cannizzo, V. T. Pham, F. van Mourik, C. Bressler, M. Chergui, *J. Am. Chem. Soc.* **2007**, *129*, 8199 – 8206; g) O. Bräm, F. Messina, E. Baranoff, A. Cannizzo, M. K. Nazeeruddin, M. Chergui, *J. Phys. Chem. C* **2013**, *117*, 15958 – 15966; h) L. S. Forster, *Coord. Chem. Rev.* **2006**, *250*, 2023 – 2033.

[19] a) A. Juris, V. Balzani, F. Barigelletti, S. Campagna, P. Belser, A. Vonzelewsky, *Coord. Chem. Rev.* **1988**, *84*, 85 – 277; b) P. S. Wagenknecht, P. C. Ford, *Coord. Chem. Rev.* **2011**, *255*, 591 – 616.

[20] F. M. Qing Pan, J. P. Korterik, D. Sharma, J. L. Herek, J. G. Vos, W. R. Browne, A. Huijser, *J. Phys. Chem. C* **2014**, *118*, 20799 – 20806.

[21] a) M. Ikuta, Y. Yuasa, T. Kimura, H. Matsuda, T. Kobayashi, *Phys. Rev. B* **2004**, *70*, 214301; b) A. T. N. Kumar, F. Rosca, A. Widom, P. M. Champion, *J. Chem. Phys.* **2001**, *114*, 701 – 724.

[22] F. Duschinsky, *Acta Physicochim. URSS* **1937**, *7*, 511.

[23] a) S. A. Kovalenko, A. L. Dobryakov, J. Ruthmann, N. P. Ernsting, *Phys. Rev. A* **1999**, *59*, 2369 – 2384; b) B. Dietzek, T. Pascher, V. Sundstrom, A. Yartsev, *Laser Phys. Lett.* **2007**, *4*, 38 – 43.

[24] a) U. Megerle, I. Pugliesi, C. Schriever, C. F. Sailer, E. Riedle, *Appl. Phys. B* **2009**, *96*, 215 – 231; b) S. A. Kovalenko, N. P. Ernsting, J. Ruthmann, *Chem. Phys. Lett.* **1996**, *258*, 445 – 454; c) D. Polli, M. R. Antognazza, D. Brida, G. Lanzani, G. Cerullo, S. De Silvestri, *Chem. Phys.* **2008**, *350*, 45 – 55.